Tuned Transition from Quantum to Classical for Macroscopic Quantum States

A. Fedorov,[1,*] P. Macha,[2,1] A. K. Feofanov,[3,1] C. J. P. M. Harmans,[1] and J. E. Mooij[1]

[1]*Kavli Institute of Nanoscience, Delft University of Technology, PO Box 5046, 2600 GA Delft, The Netherlands*

[2]*Institute of Photonic Technology, P.O. Box 100239, D-07702 Jena, Germany*

[3]*Physikalisches Institut and DFG Center for Functional Nanostructures (CFN) Karlsruhe Institute of Technology, Wolfgang-Gaede-Straße 1, D-76131 Karlsruhe, Germany*

(Received 9 December 2010; published 29 April 2011)

The boundary between the classical and quantum worlds has been intensely studied. It remains fascinating to explore how far the quantum concept can reach with use of specially fabricated elements. Here we employ a tunable flux qubit with basis states having persistent currents of 1 μA carried by a million pairs of electrons. By tuning the tunnel barrier between these states we see a crossover from quantum to classical. Released from nonequilibrium, the system exhibits spontaneous coherent oscillations. For high barriers the lifetime of the states increases dramatically while the tunneling period approaches the phase coherence time and the oscillations fade away.

DOI: 10.1103/PhysRevLett.106.170404 PACS numbers: 03.65.Ta, 03.67.Lx, 85.25.Cp

The quantum nature of quarks and atoms is as solidly established as the relevance of Newtonian mechanics for marbles and soccer balls. The boundary between the two worlds has been studied theoretically [1]. It has been also demonstrated that objects containing many atoms, such as large molecules and magnetic particles [2] or fabricated superconducting circuits [3,4] can behave like single quantum particles. In this Letter we performed an experiment on a superconducting flux qubit, which is the ''classical'' example of a macroscopic object that can be made to behave as a quantum particle. It is characterized by two states with opposite macroscopic currents in a loop [5,6]. We were able to control the tunnel barrier between these states over a very wide range. We tuned qubit energy levels below the barrier and the same time effectively cool the sample to near zero temperature. This allowed us to study the qubit behavior when we go from the range of low barriers and strong quantum tunneling to the regime where quantum tunneling gradually disappears as the barrier is increased. In particular, we manage to observe the natural quantum oscillations manifested in the tunneling of the long-living macroscopic magnetic moments. At very high barriers we see the how these oscillations fade away as the barrier is increased.

The flux qubit has a potential energy which consists of two degenerate wells [Fig. 1(a)] separated by a barrier E_B. Each well is connected with a macroscopic magnetic flux, with a sign $(+ / -)$ depending on being in the left or the right well, which can be detected on demand by a measurement apparatus. The zero-point energy E_0 of the qubit in each well can be made smaller than E_B [7,8]. Consequently, the barrier between the wells becomes classically impenetrable, and at low temperature the magnetic moment of the qubit can be flipped only via the quantum tunneling process. This process is represented in Fig. 1(a) by the tunneling coupling Δ, which depends exponentially on the barrier height E_B. To probe the quantum nature of the qubit we use the ''real-time'' experiment proposed by Leggett [1]: prepare the system in one well, let the system evolve for a time t, and measure the magnetic flux with the detector. The resulting quantum mechanical probability to find the system in the initial well equals $P(t) = (1 + \cos(2\pi\Delta t))/2$. Observation of the magnetic flux oscillations has never been reported up to now. Two earlier experiments which used similar measurement protocols for superconducting qubits in the charge [3] and phase [9] regimes. In the former case the oscillations were attributed to tunneling of a single Cooper pair. In the latter one the quantum oscillations were observed between states without

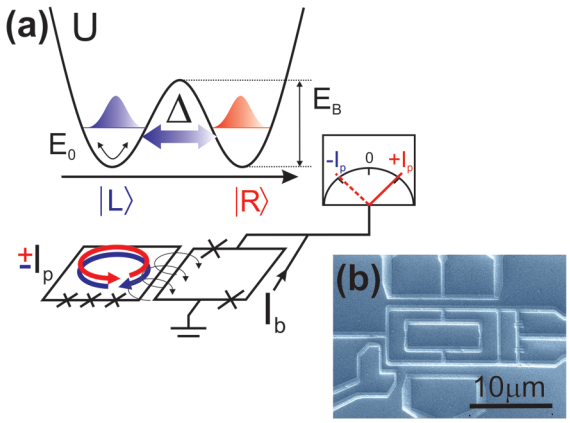

FIG. 1 (color online). Experiment to test macroscopic quantum coherence: (a) Potential energy of the flux qubit. The barrier height E_B is large compared to the zero-point energy E_0 resulting in the strong localization of states $|L\rangle$ and $|R\rangle$ which are connected to macroscopically distinguishable magnetic moments induced by the persistent currents in the qubit loop. The tunneling $|L\rangle \leftrightarrow |R\rangle$ can be observed by a DC-SQUID sensitive to a change of the magnetic flux. (b) Scanning electron micrograph of the flux qubit.

a macroscopic variable. In a flux qubit experiment a qualitatively different behavior for different tunnel barriers was attributed to the quantum and classical regimes [10].

Our flux qubit consists of three junctions symmetrically attached to a trap loop as shown in Fig. 2(a). The central junction is made tunable by replacing it by two junctions in parallel, thus providing control over E_B and so Δ. The trap loop is employed to capture a fluxoid (or 2π-phase-winding number) [11], establishing a π phase drop over the qubit junctions. If one fluxoid is trapped and the difference in flux in the two loop halves of the gradiometer $2f_\varepsilon\Phi_0 = (f_1 - f_2)\Phi_0 \approx 0$ the system has a double-well potential [Fig. 1(b)]. Here Φ_0 is the magnetic flux quantum $h/(2e)$ and $f_{\varepsilon,1}$, $f_{\varepsilon,2}$ are the fluxes in units of Φ_0. The ground states in each well of the potential are persistent current states $|L\rangle$ and $|R\rangle$ characterized by the currents $\pm I_p$ carried by the junctions, generating the before mentioned $+/-$ magnetic moments [Fig. 2(a)]. The energy eigenstates of the qubit are linear superpositions of $|L\rangle$ and $|R\rangle$ [Fig. 2(c)], following the Hamiltonian

$$H = -\frac{h}{2}(\varepsilon(f_\varepsilon, f_\alpha)\sigma_z + \Delta(f_\alpha)\sigma_x), \qquad (1)$$

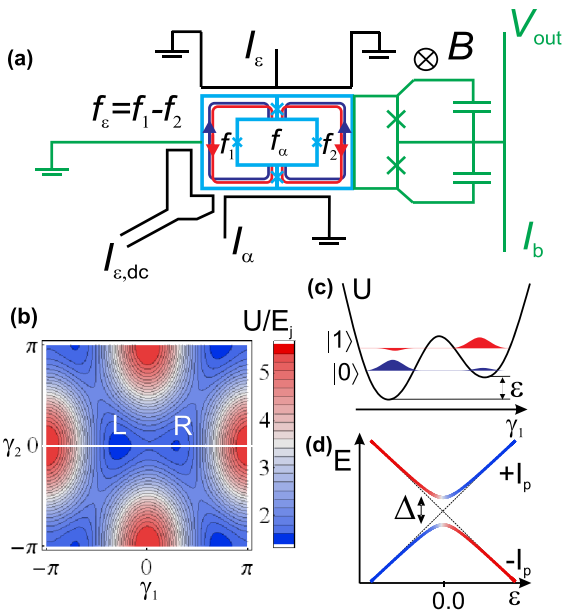

FIG. 2 (color online). Tunable flux qubit: (a) Schematics. The qubit is formed by three Josephson junctions one of which is a tunable double junction. The arrowed lines show the persistent currents connected to the states $|L\rangle$ and $|R\rangle$. The qubit state can be controlled by the bias lines I_ε, $I_{\varepsilon,dc}$, I_α and measured by the DC-SQUID. (b) Potential energy (in units of the Josephson energy of the regular junctions) as a function of the two independent phase differences γ_1 and γ_2. (c) Sketch of the cross section of the potential energy along the white line connecting left and right wells through the saddle point [see (b)]. The energy eigenstates $|0\rangle$ and $|1\rangle$ are superpositions of the persistent current states $|L\rangle$ and $|R\rangle$. (d) Energy diagram of the qubit vs magnetic bias ϵ.

where $h\varepsilon = 2I_p f_\varepsilon \Phi_0$ is the magnetic energy bias and $\sigma_{x,z}$ are Pauli matrices. The critical currents of the four junctions are designed such that the two parallel junctions each have half the value of the critical current $I_0 \simeq 700$ nA of the other two junctions. Applying *in situ* flux $f_\alpha\Phi_0$ to the parallel junctions sets their total effective critical current to $I_0\cos(\pi f_\alpha)$, in this way allowing f_α to control E_B and Δ [12]. Qubit excitation is obtained by the magnetic field generated by current in the symmetrically-split I_ε line, acting on the qubit flux $f_\varepsilon\Phi_0$. Similarly, the line I_α together with the homogeneous field B generated by an external coil, sets $f_\alpha\Phi_0$ and changes Δ. The geometrical symmetry leads to independent control of ε and Δ. The qubit states are detected with a DC-SQUID which is coupled to the qubit by a shared wire with a mutual qubit-SQUID inductance $M \simeq 6$ pH.

Figure 3(a) shows the gap of the qubit for different f_α and deduced from spectroscopy performed with the following protocol. First we set Δ with the field B and apply a dc current $I_{\varepsilon,dc}$ to have $\nu_{qb} \equiv (\Delta^2 + \varepsilon^2)^{1/2} \sim 9$ GHz. In the second step we apply a square current pulse I_ε, shifting the qubit frequency, combined with a microwave excitation. Next, the qubit is returned to $\nu_{qb} = 9$ GHz and a short bias current pulse I_b is applied to the SQUID to measure the qubit state. The relative populations of the qubit ground and excited states determine the expectation value of the

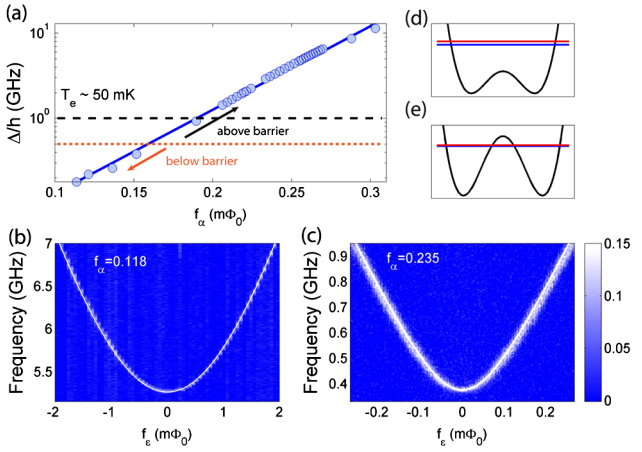

FIG. 3 (color online). Qubit properties. (a) Gap vs magnetic frustration f_α. The solid line is a guide to the eye with exponential dependence of Δ on f_α. The dashed line indicates the expected thermal noise level of 50 mK; the dotted line shows the border between formally quantum tunneling (qubit energies are below the tunnel barrier) and quantum scattering (energies are above the barrier) regimes. (b) Spectrum of the qubit in the regular regime for $\Delta = 5.2$ GHz. The white line is a fit with $I_p = 544$ nA. (c) Spectrum of the qubit in the deep tunneling regime for $\Delta = 375$ MHz. The white line shows a fit with $I_p = 344$ nA. (d),(e) numerical simulations of the double-well potential and the two lowest states corresponding to the spectra (b) and (c). The color scale represents the SQUID switching probability minus 0.5.

persistent current, resulting in a change of the SQUID switching probability (color scale) [13]. The measurement sequence is repeated a few thousand times to improve signal statistics.

The sequence starts at $\nu_{qb} \sim 9$ GHz, far above the effective noise temperature $T_e \sim 50$–100 mK (~ 1–2 GHz) and the cryostat base temperature $T_b \cong 20$ mK. After waiting for a long enough time the qubit relaxes to its ground state. During later operations the qubit splitting can be reduced to values below T_e or even T_b. With the ability of producing fast energy shifts we achieved coherent control of the qubit even for very small energy splittings for a duration limited by the relaxation time T_1. Coherent transitions below the thermal energy have been realized previously in superconducting qubits only with active microwave pulses [8,14,15] similar to laser cooling used in atomic systems and spin qubits [16].

In Fig. 3(a) one can see that the gap covers nearly two decades, ranging from 150 MHz to 12 GHz. Over the same f_α range I_p varies from 600 to 150 nA. Figures 3(b) and 3(c) show spectra for two representative cases. For the regular flux qubit gap range ($\Delta \sim 2$–10 GHz) our numerical simulations show that the qubit ground state level lies above the barrier for the double-well potential [Figs. 3(b) and 3(d)]. Only when $\Delta < 500$ MHz the qubit levels fall below the barrier and the transitions between the wells become classically forbidden [Figs. 3(c) and 3(e)]. Note that Δ closely follows an exponential dependence on f_α over the full range of Δ, a feature exclusively associated with quantum tunneling.

In order to demonstrate the emergence of the classical opaqueness of the barrier we measured the relaxation time

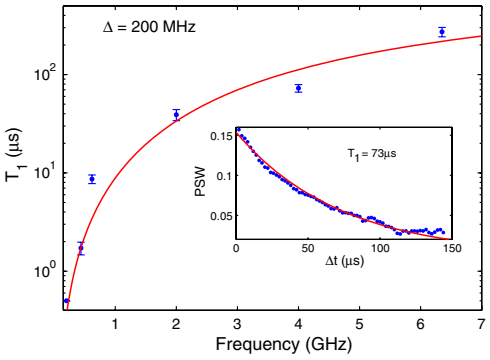

FIG. 4 (color online). Energy relaxation time T_1 vs qubit frequency ν_{qb} at $\Delta = 200$ MHz. The dots show T_1 obtained by fitting to the experimental traces measured at each qubit frequency. The error bars are the confidence intervals of the fits. The line indicates the expected relative dependence $T_1^{-1} \propto \cos^2\theta \nu_{qb} \coth(h\nu_{qb}/2k_BT_e)$ with $\tan\theta \equiv \Delta/\varepsilon$ with the absolute magnitude being a fit parameter. The noise was assumed to be Ohmic with $T_e = 50$ mK. The inset shows the actual data trace for $\nu_{qb} = 4$ GHz with $T_1 = 73$ μs (the line is fit to the measurement data). *PSW* is the switching probability of the SQUID minus 0.5.

for a small gap $\Delta = 200$ MHz as a function of ν_{qb} [Fig. 4]. From (1) it follows that $|0\rangle(|1\rangle) \propto [1 + (-)\cos\theta]|L\rangle + \sin\theta|R\rangle$, where $\tan\theta \equiv \Delta/\varepsilon$. Thus starting from $\nu_{qb} = \Delta$ the energy eigenstates are gradually transformed from (anti)symmetric superpositions of $|L\rangle$ and $|R\rangle$ states to being almost purely $|L\rangle$ and $|R\rangle$ at $\nu_{qb} = 6$ GHz $\gg \Delta$. The measurement shows a nearly 3 orders of magnitude increase in lifetime of the excited state for the localized state $|R\rangle$ compared to the delocalized superposition $(|L\rangle - |R\rangle)/\sqrt{2}$, reaching hundreds of μs. These high values of T_1 demonstrate the extreme robustness of the persistent currents.

We used the experimental sequence shown in Fig. 5(a) for time-resolved detection of macroscopic quantum coherence. We start by tuning Δ below 300 MHz with the magnetic field B to enter the deep tunneling regime. Using $I_{\varepsilon,dc}$ we also tilt the double-well potential, preparing the qubit in $|L\rangle$ with $\nu_{qb} = 4$–7 GHz. Subsequently, the double well is made symmetric by means of a fast I_ε pulse; in 0.3 ns the qubit is taken to its symmetry point. As the qubit energy changes fast relative to the tunneling amplitude Δ, this transfer is nonadiabatic thus preserving the initial state occupation. These operations lead to the situation described in Fig. 1, where the system is prepared in one of the wells of the symmetric double-well potential with a classically impenetrable barrier. The qubit is kept here for a time t, then returned fast to the 7 GHz level and finally read out to complete the "real-time"

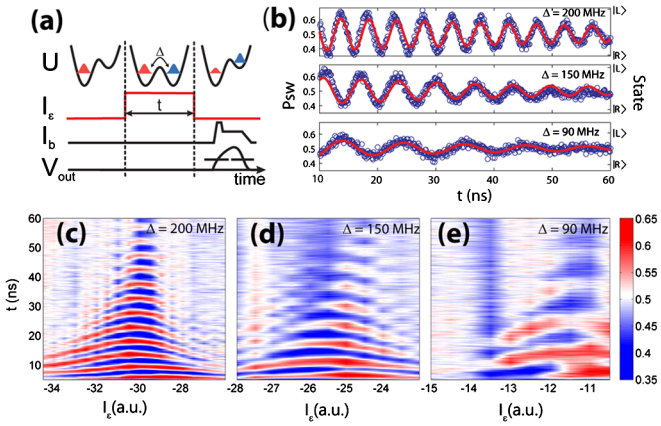

FIG. 5 (color online). Macroscopic quantum coherence of the persistent current states. (a) Measurement protocol: preparation of the qubit in $|L\rangle$ by strongly tilting the double-well potential; a fast shift to the symmetry point (symmetric double well); free evolution for time t and a fast shift back followed by the SQUID measurement pulse. (b) Time-resolved measurement of the tunneling of the persistent current states for $\Delta = 200$, 150, and 90 MHz (circles) and fit to $e^{-t/T_2}\cos(\Delta t)$ (line) with $T_2 = 65$, 45, and 35 ns, respectively. (c)–(e) The colors indicate the switching probability of the SQUID. The horizontal scale represents the amplitude of the current pulse I_ε sweeping the qubit through the symmetry point where the macroscopic quantum coherence oscillations are observed.

experiment [1]. The resulting macroscopic quantum oscillations are shown in Fig. 5(b) for successively increased tunnel barrier. In Figs. 5(c)–5(e) we swept both the length and the amplitude of the I_ε pulse.

As the barrier is raised the oscillations become slower, as expected from the corresponding decrease in the tunnel coupling Δ. The oscillation decay is caused by dephasing of the system and is characterized by the dephasing time T_2. The longest decay time is achieved around the symmetry point where the influence of the low frequency flux noise in f_ε is suppressed [17]. With higher barriers the sensitivity to low frequency flux noise increases and the phase coherence decays faster. The slowest oscillations are observed for $\Delta = 90$ MHz (i.e., an energy splitting equivalent to only 4 mK). Here the oscillation period approaches the dephasing time, thus showing the border between quantum and classical regime. A further increase of the barrier leads to a total destruction of the quantum phase between the persistent current states and the system is nolonger regarded as quantum. It is interesting to note that, for small gaps, sensitivity to f_α noise is strongly suppressed, and so the environment automatically chooses the basis of the macroscopic current states for dephasing.

Our measurements show how the flux qubit can be gradually tuned from the quantum to the classical regime. With the increase of the tunnel barrier the ''quantumness'' of the system manifested in coherent tunneling is gradually lost. At the same time the lifetime of the persistent currents dramatically increases, which is naturally associated with macroscopic classical systems or classical bits. Also, over a large range of parameters the quantum and macroscopic properties are shown to coexist. Our experiment demonstrates the potential of fabricated quantum objects, where knobs are available to tune parameters *in situ*, for fundamental research as well as for applications.

We thank R. N. Schouten for technical support. This work was supported by the Dutch NanoNed program, the Dutch Organization for Fundamental Research (FOM), and the EU projects EuroSQIP, CORNER, and SOLID.

*fedoroar@phys.ethz.ch
Present address: Department of Physics, ETH Zurich, CH-8093, Zurich, Switzerland.

[1] A. J. Leggett, J. Phys. Condens. Matter **14**, R415 (2002); A. J. Leggett and A. Garg, Phys. Rev. Lett. **54**, 857 (1985).
[2] M. Arndt, Nature (London) **401**, 680 (1999); L. Thomas, Nature (London) **383**, 145 (1996); J. R. Friedman, M. P. Sarachik, J. Tejada, and R. Ziolo, Phys. Rev. Lett. **76**, 3830 (1996).
[3] Y. Nakamura, Yu. A. Pashkin, and J. S. Tsai, Nature (London) **398**, 786 (1999).
[4] A. Palacios-Laloy *et al.*, Nature Phys. **6**, 442 (2010); M. Ansmann *et al.*, Nature (London) **461**, 504 (2009).
[5] The currents of $\sim 0.5\ \mu$A are generated by roughly 10^6 Cooper pairs. The difference between the two current states is $\sim 0.01\Phi_0$ in magnetic flux or $\sim 10^6$ Bohr magnetons. The number of corresponding orthogonal microscopic states is discussed in Ref. [6].
[6] J. I. Korsbakken, F. K. Wilhelm, and K. B. Whaley, Europhys. Lett. **89**, 30003 (2010).
[7] C. H. van der Wal *et al.*, Science **290**, 773 (2000); J. R. Friedman, V. Patel, W. Chen, S. K. Tolpygo, and J. E. Lukens, Nature (London) **406**, 43 (2000).
[8] V. E. Manucharyan, J. Koch, M. Brink, L. I. Glazman, and M. H. Devoret, arXiv:0910.3039.
[9] S. Poletto *et al.*, New J. Phys. **11**, 013009 (2009).
[10] M. Grajcar, A. Izmalkov, and E. Il'ichev, Phys. Rev. B **71**, 144501 (2005).
[11] J. Majer, J. Butcher, and J. E. Mooij, Appl. Phys. Lett. **80**, 3638 (2002).
[12] F. G. Paauw, A. Fedorov, C. J. P. M Harmans, and J. E. Mooij, Phys. Rev. Lett. **102**, 090501 (2009).
[13] P. Bertet *et al.*, Phys. Rev. Lett. **95**, 257002 (2005).
[14] S. O. Valenzuela *et al.*, Science **314**, 1589 (2006).
[15] M. Grajcar *et al.*, Nature Phys. **4**, 612 (2008).
[16] I. Bloch, Nature (London) **453**, 1016 (2008); J. R. Petta *et al.*, Science **309**, 2180 (2005).
[17] See supplemental material at http://link.aps.org/supplemental/10.1103/PhysRevLett.106.170404 for an analysis of decoherence for the flux qubit with tunable gap. The regime of low gaps is discussed in detail.